



Decomposition of the mixed-metal coordination polymer—A preparation route of the active Ag/Yb₂O₃ catalyst for the deN₂O process



Marcin Konkol ^{a, **}, Małgorzata Kondracka ^a, Paweł Kowalik ^a, Wiesław Próchniak ^a, Kamila Michalska ^a, Alexander Schwedt ^b, Carina Merkens ^c, Ulli Englert ^{c,*}

^a New Chemical Syntheses Institute (INS), Al. Tysiąclecia Państwa Polskiego 13A, 24 110 Puławy, Poland

^b Gemeinschaftslabor für Elektronenmikroskopie, RWTH Aachen University, Ahornstr. 55, 52074 Aachen, Germany

^c Institute of Inorganic Chemistry, RWTH Aachen University, Landoltweg 1, 52074 Aachen, Germany

ARTICLE INFO

Article history:

Received 9 December 2015

Received in revised form 23 February 2016

Accepted 27 February 2016

Available online 2 March 2016

Keywords:

N₂O decomposition

Mixed-metal polymers

Thermal decomposition

Ag nanoparticles

Powder diffraction

Scanning electron microscopy

Sintering

ABSTRACT

Ag nanoparticles in a Yb₂O₃ matrix catalyzed the direct decomposition of N₂O to the elements. Our investigations included X-ray powder diffraction and electron microscopy; they revealed a remarkable dependence of the catalytic activity on the catalyst preparation method that influenced the size of Ag crystallites. Simple precipitation followed by calcination resulted in the formation of a catalyst with rather large Ag crystallites, which showed low activity. In contrast, thermal decomposition of the mixed-metal Ag–Yb coordination polymer provided the Ag/Yb₂O₃ catalytic system with distinctly smaller Ag crystallites. The coordination-polymer derived catalyst exhibited much higher activity in the deN₂O process at moderate temperature range 400–500 °C.

© 2016 Elsevier B.V. All rights reserved.

1. Introduction

N₂O is one of the most important greenhouse gases with significant global warming potential (GWP) when compared to carbon dioxide (CO₂) and methane (CH₄). Due to its long lifetime of up to 140 years in the atmosphere, the greenhouse potential of N₂O is 300 times higher than that of CO₂ [1]. N₂O also causes ozone depletion, and it has been suggested that N₂O currently represents the single most important ozone-depleting substance emitted [2]. The N₂O concentration in the atmosphere increases by ca. 0.2–0.3% per year. Albeit N₂O is produced also naturally in the soil during the microbial processes of nitrification and denitrification, the observed increase is mainly caused by anthropogenic activities such as adipic acid production, nitric acid manufacture, fossil fuels and biomass combustion or land cultivation [1]. The reduction of N₂O emission from industrial sources plays a crucial role in the

overall reduction of greenhouse gases emission. For those processes in which N₂O formation is inevitable, its abatement can be achieved either by improving the selectivity of the applied catalysts or by downstream direct decomposition of N₂O into nitrogen and oxygen [1].

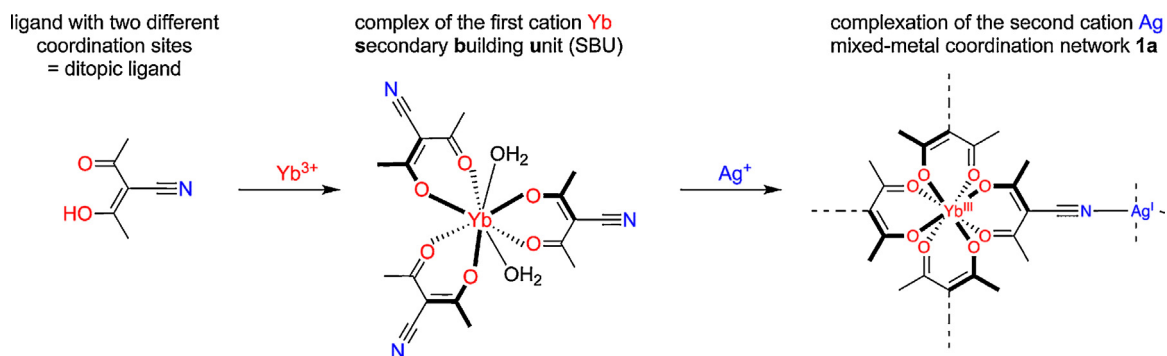
Many catalysts have been established for the latter strategy, the direct decomposition of N₂O; these catalysts comprise supported or unsupported noble metals, pure oxides, mixed oxides, spinels, perovskites and zeolites. The review by Kapteijn et al. provides a comprehensive overview on the decomposition of nitrous oxide over solid catalysts [1]. Among pure oxides, the highest activities have been reported for oxides of group VIII transition metals (Rh, Ir, Co, Fe, Ni) and for rare-earth oxides (La₂O₃) [3–5]. Several reports have shown the catalytic potential of alternative rare-earth metal oxides, Ln₂O₃ (Ln = e.g. Nd, Dy, Er) in the direct decomposition of N₂O [6–8].

Silver is known as a catalyst for the selective oxidation of methanol, and the epoxidation of ethylene. There are literature reports showing that N₂O decomposition is activated on atomically clean Ag(1 1 1) [9]. The catalytic activity of silver-based catalysts for the removal of NO_x from exhausts, both via catalytic reduction and direct decomposition, has been also intensively studied

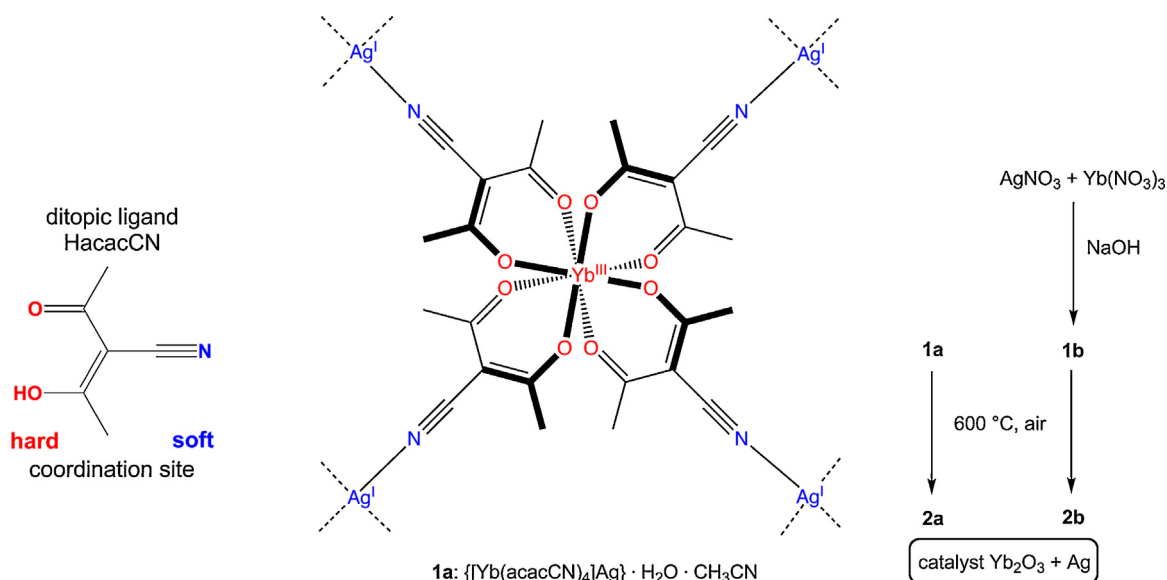
* Corresponding author.

** Corresponding author.

E-mail addresses: marcin.konkol@ins.pulawy.pl (M. Konkol), ullrich.englert@ac.rwth-aachen.de (U. Englert).



Scheme 1. Stepwise approach to a catalyst precursor: starting from a ditopic ligand, a secondary building unit is formed and crosslinked to a mixed-metal coordination network.



Scheme 2. Synthesis routes for the preparation of catalysts **2a** and **2b**.

[10–13]. Moreover, N_2O decomposition has been investigated by Ramnani et al. on SiO_2 supported nano-Ag [14] and by Angelidis and Tzitzios on $\text{Ag}/\text{Al}_2\text{O}_3$ [15] catalysts. Gac et al. reported that the presence of silver enhances to some extent the activity of cryptomelane type manganese oxide catalysts in N_2O decomposition at low temperatures [16]. Nevertheless, studies on direct decomposition of N_2O over silver-based catalysts remain relatively scarce [17]. Only recently, a combined nano-Ag/5% Al_2O_3 /1% La_2O_3 catalytic system has been reported as an efficient catalyst for direct N_2O decomposition, and the enhancement of the catalytic activity by addition of La_2O_3 has been demonstrated [18].

Metals and their oxides of high dispersion can be prepared from inorganic precursors. The object of our investigations is a catalytic system comprising silver and ytterbium(III) oxide that can be prepared *via* thermal decomposition of well-ordered bimetallic coordination networks. Such coordination networks can be obtained in a rational way following the secondary building unit (SBU) strategy [19–21] shown in Scheme 1.

We have shown in earlier contributions how suitable ditopic ligands can be employed to synthesize mononuclear transition metal [22–26], main group metal [24,27] and lanthanide [28,29] SBUs and how these SBUs may be cross-linked to extended structures. In this contribution we report the syntheses, characterization and activity of ex-coordination polymer and ex-hydroxide $\text{Ag}/\text{Yb}_2\text{O}_3$ catalysts in direct N_2O decomposition at temperatures from 25 to 800 °C.

2. Experimental

2.1. Chemicals

The ditopic ligand HacacCN was prepared from freshly distilled acetylacetone according to the literature [30]. The catalyst precursor **1a** was synthesized as described earlier [27]. All chemicals were used without further purification: $\text{Yb}(\text{NO}_3)_3 \cdot 5\text{H}_2\text{O}$ (98.5%, Aldrich) and AgNO_3 (99.5%, KMF Laborchemie).

2.2. Catalyst preparation

Catalyst **2a**

50 mg of the catalyst precursor **1a** was placed in a glazed porcelain boat and introduced into a horizontal tube furnace. The sample was heated to 600 °C in air over a period of 40 min. This temperature was maintained for 30 min and the sample was then allowed to cool to ambient temperature. The residue corresponded to 17 mg of catalyst **2a**.

Catalyst **2b**

Separate equimolar solutions of the metal nitrates were prepared: 1.795 g (5 mmol) of $\text{Yb}(\text{NO}_3)_3$ and 0.849 g (5 mmol) of AgNO_3 were dissolved each in 25 mL of deionized water. The solutions were combined and 1 molar solution of NaOH in deionized water was added dropwise until no further precipitate formed. The solid was recovered by filtration, washed from unwanted ions until a

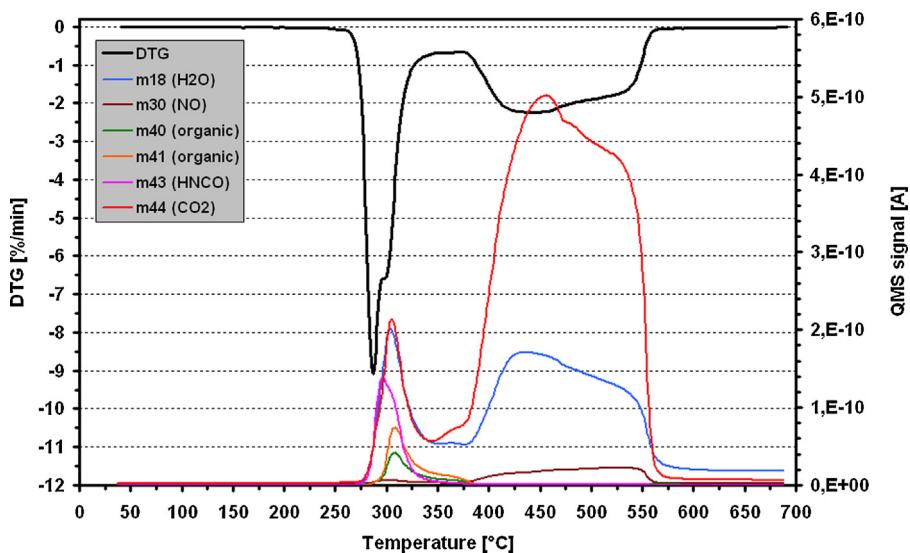


Fig. 1. DTG and S_{QMS} curves for **1a** in air.

filtrate conductivity below $100 \mu\text{S}$ was reached and dried overnight in a desiccator. It was then placed in a glazed porcelain crucible and calcined as above.

2.3. Catalyst characterization

The chemical composition of the samples was determined by means of the XRF method using an X'UNIQUE II – Philips spectrometer. X-ray powder diffraction experiments including quantitative phase analysis and crystallite size studies were performed on a PANalytical Empyrean system (Bragg-Brentano geometry) equipped with a PIXcel^{3D} detector using Cu K α radiation and operating at 40 kV and 40 mA. The samples were scanned between $8 < 2\theta < 70^\circ$ (2θ region 25 – 70° is shown for clarity), with the step size 0.01° . The X-ray diffraction patterns were analyzed with the HighScore Plus program. The patterns were refined with a sum of pseudo-Voigt profile function and an appropriate background function. The quantitative analysis of crystallographic phases was carried out by means of the semi-automatic Rietveld method. The size of Ag crystallites was estimated from the diffraction lines (1 1 1) and (2 0 0) using the Scherrer equation ($d = K\lambda/\beta\cos\theta$, where K-Scherrer equation constant = 0.9, λ —wavelength of radiation [nm], β —FWHM [rad], and θ —diffraction angle [rad]). The correction for instrumental broadening was applied with the reference standard (LaB₆). Temperature-programmed XRD measurements were carried out in an Anton Paar HTK-16N chamber. The sample was deposited as a thin layer (ca. 0.1 mm) on a Pt heating strip. A Pt/Pt-13%Rh thermocouple spot-welded to the bottom of the heating strip was used for measuring the temperature. *In situ* XRD patterns were recorded isothermally at intervals of 100°C up to the temperature of 400°C and at intervals of 50°C in the temperature range 400 – 650°C , maintaining 15 min stabilization time at each temperature.

The specific surface area of the samples was determined on the basis of BET model by measuring nitrogen adsorption at $p/p_0 = 0.05$ – 0.3 using a Micromeritics ASAP 2050 Xtended Pressure sorption analyzer. Parameters describing the porosity of the solids (in a pore size range of 2–300 nm) were determined from N₂ adsorption isotherms with the BJH method.

Thermal decomposition of the catalyst precursor was studied by TG-EGA (evolved gas analysis) in synthetic air in the temperature range of 40 – 700°C . The measurements were carried out with a STA 449 F3 Jupiter thermal analyzer coupled with a QMS 403C

Aeolos NETZSCH mass spectrometer. A sample (ca. 30 mg) was placed in a ceramic vessel mounted on a microbalance arm and then heated with a rate of $10^\circ\text{C}/\text{min}$. The following parameters were recorded: temperature (T [$^\circ\text{C}$]), mass loss of the analyzed sample (DTG [%/min]) and mass signals (S_{QMS} [A]) coming from the volatile products evolved from the sample: H₂O ($m/q = 18$), N₂ or CO ($m/q = 28$), NO ($m/q = 30$), HNCO ($m/q = 43$), CO₂ ($m/q = 44$).

Scanning electron microscopy (SEM) was used in order to analyze the surface morphology and tendency to recrystallization and agglomeration of the particles. Depending on the focus of the analysis, two different field-emission gun (FEG-)SEMs were used. High-resolution secondary electron (SE) images of the surface topography were obtained using a DSM 982 Gemini instrument by Zeiss, equipped with an in-lens SE detector, at low electron energies (typically 4 keV) and low working distances (typically 3 mm). Backscatter electron (BSE) imaging and energy-dispersive X-ray (EDX) analyses were performed in order to get information about the chemical homogeneity on the microscale using a JSM7000F instrument by JEOL, equipped with an YAG-BSE detector by Autrata and a Sapphire Si(Li)-EDX detector by Ametek-EDAX. These analyses were performed using a beam energy of 15 keV at the optimum analytical working distance of the EDX detector of 10 mm. Prior to analyses, for selected samples a small amount of powder was embedded in a conductive resin ('WEM-REM' by Schmitz Metallographie), and subsequently cross-sections through the particles were prepared using ion polishing in a cross-section polisher SM-09010 by JEOL, operated with 6 keV Ar⁺-ions.

2.4. Activity evaluation

The evaluation of the catalytic activity in N₂O decomposition was carried out in a gradientless fixed-bed reactor under atmospheric pressure [31]. The gradientless effect in this reactor was achieved through back diffusion across a thin layer of fine-grained catalyst (100 mg, grain size <0.16 mm, layer thickness below 2 mm). The measurements were conducted in the temperature range 25 – 800°C with a rate $100^\circ\text{C}/\text{h}$. The stabilization time at each temperature was 1 h. The reactor was fed with a stream of N₂O/NO in N₂ via a mass flow controller. The inlet NO content was 900 ppm, N₂O 1400 ppm, the process gas flow rate was 4–6 Ndm³/h. The outlet gas was analyzed for N₂O concentration using an optical Gasmet analyzer.

The N_2O conversion degree was calculated based on the following formula: $X_{\text{N}_2\text{O}} = (\text{C}_0 - \text{C}_1)/\text{C}_0$, where C_0 — N_2O inlet concentration [ppm], C_1 — N_2O outlet concentration [ppm]. During the calculations of $r_{\text{N}_2\text{O}}$ and $k_{\text{N}_2\text{O}}$, an effect of contacting of reactor's walls was taken into account by adjusting the outlet N_2O concentration in a test with a loaded reactor by the value of the N_2O concentration in a test conducted on the empty reactor (other parameters were constant). The reaction rate $r_{\text{N}_2\text{O}}$ was calculated from the equation: $r_{\text{N}_2\text{O}} = V \times X_{\text{N}_2\text{O}} \times C_0 \times 10^{-6} \times m_{\text{cat}}^{-1}$, where m_{cat} —catalyst weight [g], V —gas flow [mol/h]. As an activity measure a rate constant $k_{\text{N}_2\text{O}}$ was applied that was calculated with the following equation: $k = r_{\text{N}_2\text{O}}/p_1$, where p_1 — N_2O outlet partial pressure [ata], assuming a first-order reaction [32]. Based on the Arrhenius relationship the apparent activation energies for N_2O decomposition were estimated.

3. Results and discussion

3.1. Synthesis and thermal decomposition of precursors

In Scheme 2 two distinctly different methods for the preparation of the $\text{Ag}/\text{Yb}_2\text{O}_3$ catalytic system are compared, namely, (a) decomposition of suitable bimetallic coordination polymer (catalyst **2a**) and (b) conventional and much less demanding precipitation method followed by thermal decomposition (catalyst **2b**). Experimental details concerning the decomposition reactions are given in Section 2.1.

Route (a) requires the synthesis of an organic ligand, a secondary building block and a mixed-metal coordination polymer and is therefore much more demanding than the latter pathway (b). With regard to the first synthesis route, a two-step strategy was involved in the preparation of the bimetallic Ag - Yb coordination polymer. The ditopic ligand, 3-cyanopentane-2,4-dionate (acacCN) [30] was employed as a linker between the cations; its coordination sites obviously differ with respect to Pearson hardness [33,34]. In the first step, the chelating acetylacetone moiety, the “hard” coordination site of the ligand, was linked to the lanthanide, resulting in an intermediate mononuclear complex. This compound may be isolated as crystalline solid of the composition $[\text{Yb}(\text{acacCN})_3(\text{H}_2\text{O})_2] \cdot 2\text{H}_2\text{O}$ (Scheme 1). In the second reaction, ligand redistribution and crosslinking occur; an addition of AgPF_6 leads to neutral networks, formally consisting of Ag^+ cations attached to the peripheral “soft” nitrile groups in the $[\text{Yb}(\text{acacCN})_4]^-$ anions (Scheme 2). This precursor **1a** forms almost immediately and corresponds to a reaction product in which each Ag(I) cation is coordinated by four nitrile groups of different Yb complexes and in which each peripheral N atom in this $[\text{Yb}(\text{acacCN})_4]^-$ linker acts as a donor towards a silver cation. In this way, an interpenetrated 3D structure forms, with each substructure adopting the diamond topology. Despite the interpenetration, overall space-filling is inefficient, and the regions between the extended subnets are filled with solvent molecules acetonitrile and water. The resulting solid undergoes fast desolvation and loss of crystallinity upon removal from the mother liquor.

The **1a** precursor represents a bimetallic solid, in which Ag(I) and Yb(III) cations are arranged in a regular fashion. In order to obtain the final catalysts, **1a** was thermally decomposed at 600°C in air (Scheme 2). Powder diffraction data show that the resulting product **2a** contains (metallic) Ag and Yb_2O_3 in the C-type rare earth oxide structure.

Thermal decomposition of **1a** was investigated in more detail by a combination of thermogravimetry and mass spectrometry. The results of DTG/EGA measurements are shown in Fig. 1. The first decomposition step of the precursor **1a** is dominant and characterized by a large and violent mass loss (ca. 30 wt%) in the range

Table 1
Physicochemical data for catalysts **2a** and **2b**.

Catalyst	XRF [wt%]		S_{BET} [m^2/g]	V_c [cm^3/g]	V_{mes} [cm^3/g]
	Yb_2O_3	Ag			
2a	65.4	34.6	7.3	0.027	0.015
2b	68.0	32.0	6.0	0.024	0.017

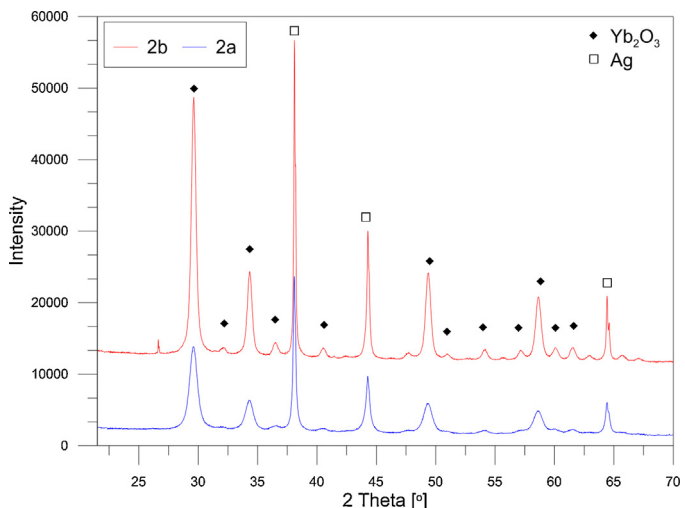


Fig. 2. XRD diffractograms of the $\text{Ag}/\text{Yb}_2\text{O}_3$ catalysts **2a** (bottom) and **2b** (top).

250–375 °C. The evolution of H_2O , CO_2 , HNCO and lower amounts of unidentified species ($m/z = 40$ and 41) was observed. The second decomposition step proceeds above 375 °C. A large mass loss (ca. 25–30 wt%) with the evolution of large amounts of CO_2 , H_2O and small amounts of NO can be observed. The intensity of this process and composition of evolved gases indicate the sample combustion in this temperature range that is usually accompanied by a high exothermic heat effect. The total mass loss at 650 °C was ca. 60 wt%.

The second synthesis route (b) consists in the joint precipitation of Ag(I) and Yb(III) by basic aqueous solution, followed by filtration, drying and calcination. It represents a simple alternative procedure for the synthesis of the $\text{Ag}/\text{Yb}_2\text{O}_3$ catalyst. By this second approach the product **2b** in Scheme 2 was obtained. Its preparation does not require any more involved organic synthesis and can therefore easily be upscaled to larger quantities.

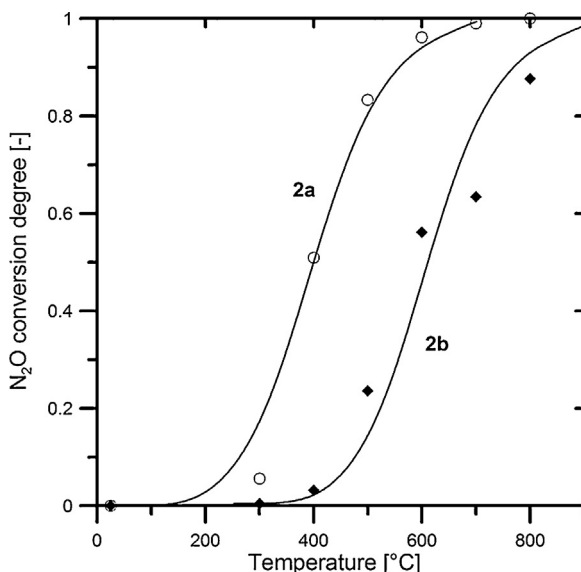
3.2. Physicochemical properties and activity of catalysts

The physicochemical properties of the $\text{Ag}/\text{Yb}_2\text{O}_3$ catalysts **2a** and **2b** were evaluated and Table 1 shows their chemical composition, specific surface area (S_{BET}), total pore volume (V_c) and volume of mesopores (V_{mes}). The results reveal that both catalysts calcined at 600 °C exhibit similar texture properties. The specific surface area and pore volume are relatively small for both samples. After calcination the dominant pores are in the range of 10–100 nm. This corresponds to structures intermediate between meso- and macroporous.

According to the XRF measurements, the contents of Ag and Yb_2O_3 in both samples under study were in the ranges 32–35 and 65–68 wt%, respectively. XRF revealed a metal Ag:Yb ratio = 1:1.06 in the solid (**2a**). The diffractograms for **2a**, obtained via decomposition of the coordination polymer **1a**, in comparison with the catalyst **2b** are shown in Fig. 2. The XRD patterns revealed the crystalline nature of catalysts and the presence of metallic Ag^0 . In both **2a** and **2b** the same two crystallographic phases were present, namely Ag (ICDD 04-002-1347) and Yb_2O_3 (ICDD 04-008-8237). For **2a** derived from the bimetallic coordination polymer, the diffraction peaks

Table 2Average crystallite size before and after N_2O decomposition tests.

Catalyst	Average crystallite size before N_2O decomposition test, d [nm]		Average crystallite size after N_2O decomposition test, d [nm]	
	Ag	Yb_2O_3	Ag	Yb_2O_3
2a	32	10	73	12
2b	95	17	>150	20

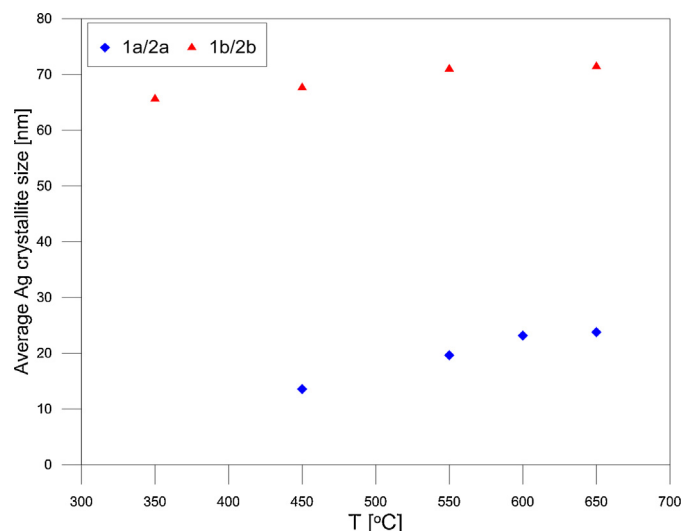
**Fig. 3.** N_2O conversion degree vs temperature for the catalysts **2a** and **2b**.

associated with the silver phase were found to be broader, indicating smaller crystallites compared to catalyst **2b**. Indeed, analysis of the crystallite size indicated that in case of **2a** the average size of silver crystallites amounted to ca. 30 nm, as shown in **Table 2**. This value is much lower than the 95 nm average size of silver crystallites in **2b**, the material prepared by precipitation and thermal treatment at 600 $^{\circ}\text{C}$. These findings prove that the decomposition of the coordination polymer results in the formation of smaller silver nanoparticles. Similarly, the average size of ytterbium oxide crystallites in **2a** was found to be lower than in the case of **2b** (10 vs 17 nm).

The catalytic activity of both Ag/Yb₂O₃ catalysts was investigated in the direct N_2O decomposition reaction in the temperature range 25–800 $^{\circ}\text{C}$. A mixture of $\text{N}_2\text{O}/\text{NO}/\text{N}_2$ was used in the tests for catalytic performance. During these experiments, the concentration of NO remained essentially constant. Thus, only N_2O conversion and no NO decomposition was observed for the Ag/Yb₂O₃ catalysts. The catalytic data are summarized in **Table 3**, the plot of reaction rate vs temperature is shown in **Fig. 3**.

The results reveal that **2a** exhibits high catalytic activity in the N_2O decomposition process at 500 $^{\circ}\text{C}$ (83% of conversion) and is still moderately active at 400 $^{\circ}\text{C}$ (51% of conversion). In contrast, **2b** shows low activity at 500 $^{\circ}\text{C}$ (23.6% of conversion). Having in mind different degrees of conversion, the reaction rate $r_{\text{N}2\text{O}}$ for **2a** at 500 $^{\circ}\text{C}$ was found to be 3.5-times higher than for **2b**. A characteristic criterion for the estimation of the catalytic activity is the temperature, at which conversion of the reactant amounts to 50%. In the case of catalyst **2a**, this temperature is 180 $^{\circ}\text{C}$ lower than that determined for the corresponding catalyst **2b** (400 vs 580 $^{\circ}\text{C}$).

Other silver-containing catalysts were reported to be active in N_2O decomposition. Tzitzios and Georgakilas found that upon addition of 3% Pd to the monometallic 5% Ag/ γ -Al₂O₃ catalyst the conversion increased from 70% to 100% at 680 $^{\circ}\text{C}$ [17]. Moreover,

**Fig. 4.** Influence of the temperature on silver crystallite size during decomposition of **1a** and **1b** precursors.

Sri Hari Kumar et al. reported N_2O conversion of ca. 43% over a 5% Ag/Al₂O₃ catalyst at a temperature of 600 $^{\circ}\text{C}$, but addition of 1% La₂O₃ enhanced the catalytic activity to 100% conversion [18]. However, in both cases no kinetic data were provided.

The significantly higher activity of **2a** compared to **2b** is somewhat surprising. Since no remarkable differences in the physicochemical properties such as specific surface area and total pore volume were found, this higher catalytic activity must be rationalized in terms of higher number of exposed silver particles or smaller silver crystallites in the former and hence higher active silver surface area. In order to further clarify differences in activity, the average size of silver crystallites after the N_2O decomposition reaction was estimated by means of the XRD method. The most active Ag/Yb₂O₃ catalyst **2a** was found to have the smallest silver crystallites after the catalytic test (ca. 73 nm), indicating a lower degree of sintering when compared to the catalyst **2b** (>150 nm). The same observations were made for ytterbium oxide, however, the differences were not that pronounced as for silver (**2a**, 12 nm; **2b**, 20 nm). Moreover, the growth of silver crystallites during decomposition/oxidation of **1a** and **1b** precursors in air was investigated in an *in situ* HT-XRD experiment. The influence of the temperature on the silver crystallite size is presented in **Fig. 4**. The results fully confirm that the decomposition of the coordination polymer **1a** provided much smaller silver crystallites in the entire temperature range. The crystallites grew upon sintering from ca. 14 nm at 450 $^{\circ}\text{C}$ to 24–25 nm at 650 $^{\circ}\text{C}$ but were still almost three times smaller than the silver crystallites upon decomposition of the precipitated precursor **1b** under the same conditions (650 $^{\circ}\text{C}$; ca. 65 nm). Furthermore, the thermal decomposition of **1b** resulted in relatively large silver crystallites already at 350 $^{\circ}\text{C}$ (ca. 66 nm) and no significant crystallite growth was observed in the temperature range 350–650 $^{\circ}\text{C}$. In a second experiment two precursor samples, **1a** and **1b**, were placed in an oven and calcined in air for 4 h at 650 $^{\circ}\text{C}$. The results of the silver crystallite size analysis again confirmed previous findings although the silver crystallites were much larger than in HT-XRD experiments due to the prolonged thermal treatment. The silver crystallites of ca. 77 nm were estimated for **1a** that emerged to be at least two times smaller than in the case of **1b** (>150 nm). Both values of silver crystallites correspond very well with those estimated after N_2O decomposition tests (vide **Table 2**).

Both catalysts exhibit similar activation energies (76.1 kJ/mol for **2a** and 83.2 kJ/mol for **2b**) as can be seen from the slope of Arrhenius plots in **Fig. 5**. This indicates that mechanism of N_2O decomposition

Table 3

The N_2O degree of conversion, reaction rates and constants for catalysts **2a** and **2b**.

T [°C]	2a			2b		
	$X_{\text{N}2\text{O}}$	$r_{\text{N}2\text{O}} [\text{mmol}_{\text{N}2\text{O}} \times \text{g}^{-1} \times \text{h}^{-1}]$	$k_{\text{N}2\text{O}} [\text{mol}_{\text{N}2\text{O}} \times \text{g}^{-1} \times \text{h}^{-1} \times \text{ata}^{-1}]$	$X_{\text{N}2\text{O}}$	$r_{\text{N}2\text{O}} [\text{mmol}_{\text{N}2\text{O}} \times \text{g}^{-1} \times \text{h}^{-1}]$	$k_{\text{N}2\text{O}} [\text{mol}_{\text{N}2\text{O}} \times \text{g}^{-1} \times \text{h}^{-1} \times \text{ata}^{-1}]$
25	0	0	0	0	0	0
300	0.06	0.173	0.13	0.005	0.004	0
400	0.51	1.585	2.30	0.03	0.101	0.07
500	0.83	2.594	11.10	0.24	0.743	0.69
600	0.96	2.993	55.44	0.56	1.760	2.86
700	0.99	3.085	242.7	0.63	2.000	3.88
800	–	–	–	0.88	2.762	15.87

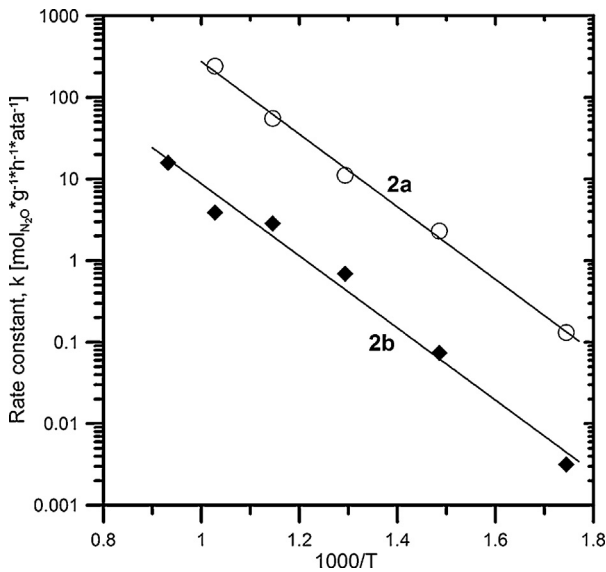


Fig. 5. Arrhenius plots for the $\text{Ag}/\text{Yb}_2\text{O}_3$ catalysts **2a** and **2b**.

are similar on both catalysts; the number of active sites is, however, significantly higher in case of **2a**.

An independent indication explaining the different activities of both catalysts under study comes from electron microscopy measurements. The ion polished cross sections of both catalysts are presented in Fig. 6. In real space, the electron microscopy confirms the diffraction results. In either catalyst, silver is still present in the form of metallic particles and a matrix, in which the silver particles are embedded, is formed with ytterbium(III) oxide. Small Ag X-ray lines in the spectra of the Yb_2O_3 matrices occur due to the much larger interaction volume of the electrons in Yb_2O_3 and do not point to a reaction between both components.

Since the components of both catalysts are chemically identical, differences have to be searched in the microstructural arrangement of the individual components within the catalysts. Fig. 7 shows a comparison of backscattered electron (BSE) images at $1000\times$ and $10000\times$ magnification. In catalyst **2b**, Ag can be found in larger particles, partly exceeding some $10\ \mu\text{m}$ in diameter. Small contributions of orientation contrasts to the BSE intensity (cf. the twinned grain marked with an arrow in the upper right image of Fig. 7) point to a polycrystalline nature of these particles with grain sizes in the range of $1\ \mu\text{m}$. The images at lower magnifications show a layered arrangement of these Ag particles between Yb_2O_3 layers of different porosity. On the contrary, in catalyst **2a** the Ag particles, dispersed

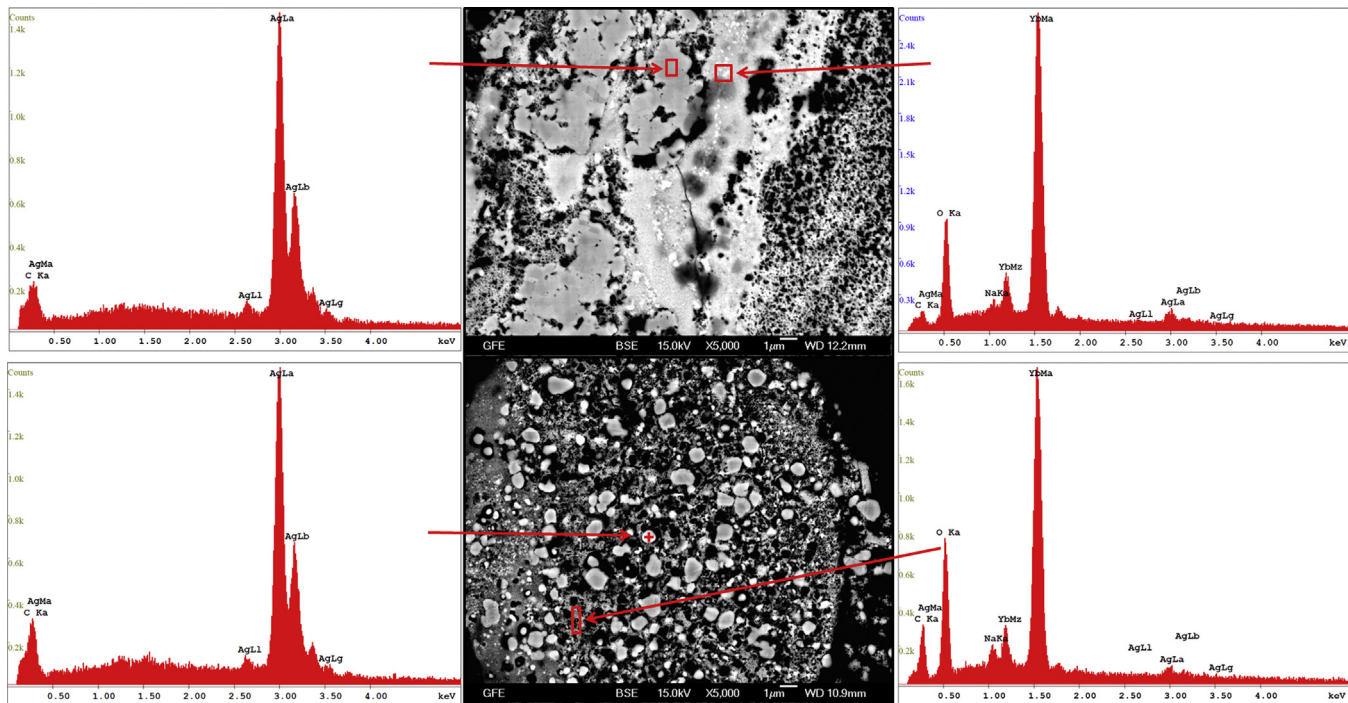


Fig. 6. EDX spectra of the components in the less efficient catalyst **2b** (top) and in the most active catalyst **2a** (bottom).

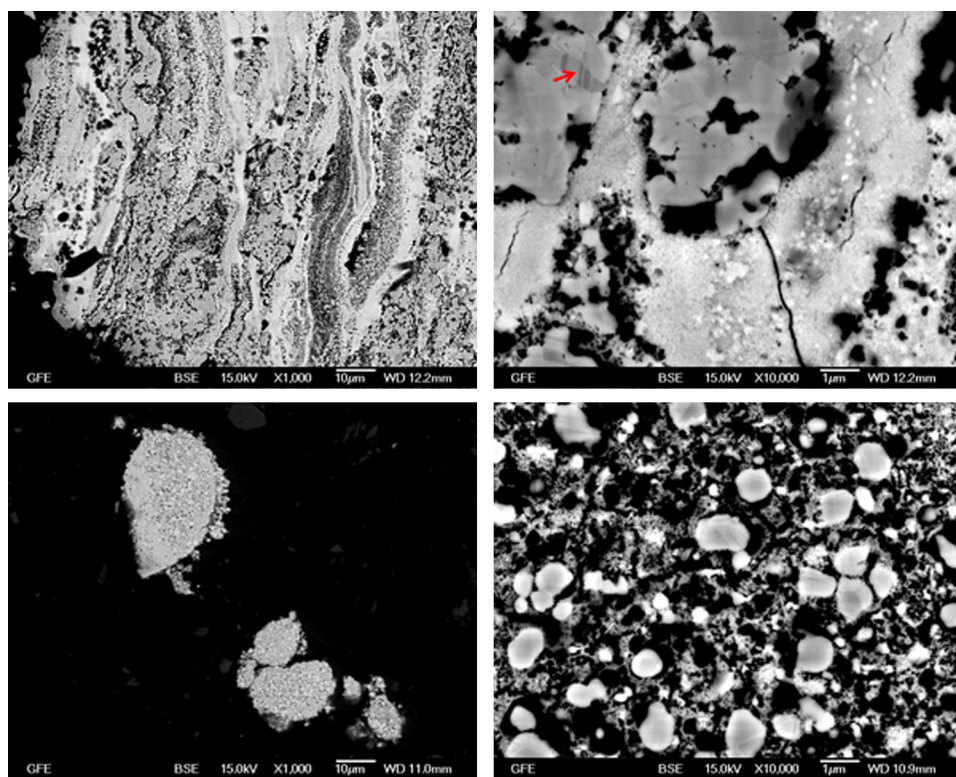


Fig. 7. Microstructure of the two catalysts at 1000x and 10000x magnification (**2b** at the top, **2a** at the bottom).

in the Yb_2O_3 matrix, have sizes of homogeneously below 1 μm . The orientation contributions to the BSE intensity show some fine twinning.

4. Conclusions

The $\text{Ag}/\text{Yb}_2\text{O}_3$ catalyst was found to exhibit high activity in direct N_2O decomposition. Catalyst obtained via thermal decomposition of a coordination polymer, i.e., a precursor containing both Ag and Yb cations in an atomic degree of dispersion, was much more active at moderate temperatures in the range 400–500 °C than the catalyst, for which the precursor was obtained by precipitation and subsequent calcination. A remarkable difference in silver crystallite sizes between these two catalysts was observed. The mixed-metal coordination polymer implies the most intimate “mixing” which can be conceived, namely an alternating sequence of Ag(I) and Yb(III) within the same unit cell; the catalyst derived by its decomposition shows very fine granularity. Thus, thermal decomposition of the bimetallic coordination polymer $[\text{Yb}(\text{acacCN})_4]\text{Ag}$, albeit much more complicated and time-consuming, is more favorable than conventional precipitation, since it leads to a final catalyst with significantly smaller silver particles which in turn results in higher activity in the N_2O decomposition reaction.

Our results demonstrate that the preparation technique remarkably determines the size of silver crystallites as well as their stability during thermal treatment and under conditions of the de N_2O process. The utilization of mixed-metals polymers may also provide other metals as stable solid dispersions useful as heterogeneous catalysts. Future work will involve the synthesis of less demanding bimetallic precursors, preferably with lower Ag content, and the study of their decomposition products.

Acknowledgements

The authors are grateful to Claudia Pütz, Ruth Harscheidt and Kevin Kistermann for the preparation of the cross-section polished specimens and to Irmgard Kalf, Friedrich Steuber and Qianqian Guo for the synthesis of the catalysts. This work was supported by the Excellence Initiative of the German federal state governments.

References

- [1] F. Kapteijn, J. Rodriguez-Mirasol, J.A. Moulijn, *Appl. Catal. B: Environ.* 9 (1996) 25–64.
- [2] A.R. Ravishankara, J.S. Daniel, R.W. Portmann, *Science* 326 (2009) 123–125.
- [3] E.R.S. Winter, *J. Catal.* 19 (1970) 32–40.
- [4] Y. Li, J.N. Armor, *Appl. Catal. B* 1 (1992) L31–L40.
- [5] X. Zhang, A.B. Walters, M.A. Vannice, *Appl. Catal. B* 4 (1994) 237–256.
- [6] E.R.S. Winter, *J. Catal.* 15 (1969) 144–152.
- [7] E.R.S. Winter, *J. Catal.* 34 (1974) 431–439.
- [8] J.F. Read, *J. Catal.* 28 (1973) 428–441.
- [9] S.A. Tan, R.B. Grant, R.M. Lambert, *J. Catal.* 104 (1987) 156–163.
- [10] K. Masuda, K. Tsujimura, K. Shinoda, T. Kato, *Appl. Catal. B: Environ.* 8 (1996) 33–40.
- [11] F.C. Meunier, V. Zuzaniuk, J.P. Breen, M. Olsson, J.R.H. Ross, *Catal. Today* 59 (2000) 287–304.
- [12] K. Masuda, K. Shinoda, T. Kato, K. Tsujimura, *Appl. Catal. B: Environ.* 15 (1998) 29–35.
- [13] T.N. Angelidis, N. Kruse, *Appl. Catal. B: Environ.* 34 (2001) 201–212.
- [14] S.P. Ramnani, S. Sabharwal, J. Vinod Kumar, K. Hari Prasad Reddy, K.S. Rama Rao, P.S. Sai Prasad, *Catal. Commun.* 9 (5) (2008) 756–761.
- [15] T.N. Angelidis, V. Tzitzios, *Ind. Eng. Chem. Res.* 42 (2003) 2996–3000.
- [16] W. Gac, G. Giecko, S. Pasieczna-Patkowska, T. Borowiecki, L. Kępiński, *Catal. Today* 137 (2008) 397–402.
- [17] V.K. Tzitzios, V. Georgakilas, *Chemosphere* 59 (2005) 887–891.
- [18] A. Sri Hari Kumar, V. Venkateswarlu, K.S. Rama Rao, N. Lingaiah, P.S. Sai Prasad, *Int. J. Chem. Phys. Sci.* 2 (2013) 114–122.
- [19] M. Eddaoudi, D.B. Moler, H. Li, B. Chen, T.M. Reineke, M. O’Keeffe, O.M. Yaghi, *Acc. Chem. Res.* 34 (2001) 319–330.
- [20] J. Kim, B. Chen, T.M. Reineke, H. Li, M. Eddaoudi, D.B. Moler, M. O’Keeffe, O.M. Yaghi, *J. Am. Chem. Soc.* 123 (2001) 8239–8247.
- [21] V.D. Vreshch, A.N. Chernega, J.A.K. Howard, J. Sieler, K.V. Domasevitch, *Dalton Trans.* (2003) 1707–1711.

- [22] M. Kondracka, U. Englert, Inorg. Chem. 47 (2008) 10246–10257.
- [23] C. Merkens, K.-N. Truong, U. Englert, Acta Crystallogr. B 70 (2014) 705–713.
- [24] C. Merkens, F. Pan, U. Englert, CrystEngComm 15 (2013) 8153–8158.
- [25] A. Wang, C. Merkens, U. Englert, CrystEngComm 17 (2015) 4293–4300.
- [26] Q. Guo, C. Merkens, R. Si, U. Englert, CrystEngComm 17 (2015) 4383–4393.
- [27] C. Merkens, U. Englert, Dalton Trans. 41 (2012) 4664–4673.
- [28] C. Merkens, N. Becker, K. Lamberts, U. Englert, Dalton Trans. 41 (2012) 8594–8599.
- [29] C. Merkens, O. Pecher, F. Steuber, S. Eisenhut, A. Görne, F. Haarmann, U. Englert, Z. Anorg. Allg. Chem. 639 (2013) 340–346.
- [30] C.M. Silvernail, G. Yap, R.D. Sommer, A.L. Rheingold, V.W. Day, J.A. Belot, Polyhedron 20 (2001) 3113–3117.
- [31] J. Zieliński, React. Kinet. Catal. Lett. 17 (1981) 69–75.
- [32] J. Kruk, K. Stolecki, K. Michalska, M. Konkol, P. Kowalik, Catal. Today 191 (2012) 125–128.
- [33] R.G. Pearson, J. Am. Chem. Soc. 85 (1963) 3533–3599.
- [34] R.G. Pearson, Chemical Hardness, Applications from Molecules to Solids, Wiley-VCH, Weinheim, 1997.